AGU ADVANCING EARTH AND SPACE SCIENCES

Geophysical Research Letters

RESEARCH LETTER
10.1029/2024GL112404

Climate Control on Erosion: Evolution of Sediment Flux From Mountainous Catchments During a Global Warming Event, PETM, Southern Pyrenees, Spain

M. Prieur[1], C. Robin[2], J. Braun[3], R. Vaucher[1], A. C. Whittaker[4], R. Jaimes-Gutierrez[1], A. Wild[3], J. S. McLeod[4], L. Malatesta[3], C. Fillon[5], F. Schlunegger[6], T. O. Sømme[7], and S. Castelltort[1]

[1]Department of Earth Sciences, University of Geneva, Geneva, Switzerland, [2]Geosciences Rennes, University of Rennes, Rennes, France, [3]Earth Surface Process Modelling, GFZ German Research Centre for Geosciences, Potsdam, Germany, [4]Department of Earth Science and Engineering, Imperial College London, London, UK, [5]Total Energies, Pau, France, [6]Institute of Geological Sciences, University of Bern, Bern, Switzerland, [7]Equinor, Fornebu, Norway

Abstract Extreme hydroclimates impact sediment fluxes from mountainous catchments to the oceans. Given modern global warming, a challenge is to assess the sensitivity of erosion in mountainous catchments to extreme climate perturbations. Here, we reconstruct paleo-sedimentary fluxes across an abrupt global warming, the Paleocene-Eocene Thermal Maximum (PETM, ~56 Ma), using sedimentary archives and numerical modeling. In the Tremp Basin (Southern Pyrenees, Spain), our results demonstrate that depositional volumetric rates of siliciclastic sediments increased two-fold during the PETM. According to the BQART and stream power law models, changes in mean annual temperature and precipitation explain only 9%–27% of the flux increase. This comparison between field data and model predictions suggests that even with high uncertainty on paleoclimate data, extreme rainfall events and landslides may have been crucial sediment generation processes during the PETM. This is consistent with predictions of enhanced climate variability in a warmer world, leading to significant sediment flushing.

Plain Language Summary Climate change has an impact on rainfall through annual precipitation and the occurrence of extreme storm events. In turn, rainfall impacts river floods, which are linked to erosion and the transport of sediments from the mountains to continental plains and, ultimately, to the oceans. Our study focuses on the excess sediments eroded from the mountains and transported to the continental plains during a climate change that occurred 56 million years ago. We found that, in the Spanish Pyrenees, this amount was, on average, multiplied by two. Numerical models suggest that the increase in mean annual temperatures and rainfall are minor triggers of the observed increase in sedimentary fluxes. This suggests that other erosion processes, for example, during extreme flood events and landslides, must occur more frequently during climate change, constituting major risks for populations in mountainous areas.

Key Points:

- Sediment fluxes are estimated from sedimentary volumes in the Tremp Basin (Spain) before and during the Paleocene-Eocene Thermal Maximum
- Sediment flux entering the basin increases by a factor of two during the warming event, indicating enhanced erosion in the catchment
- Erosion models based on mean annual rainfall and temperature changes fail to reproduce observations, hinting at the role of extreme events

Supporting Information:

Supporting Information may be found in the online version of this article.

Correspondence to:

M. Prieur,
m.prieur.t@gmail.com

Citation:

Prieur, M., Robin, C., Braun, J., Vaucher, R., Whittaker, A. C., Jaimes-Gutierrez, R., et al. (2025). Climate control on erosion: Evolution of sediment flux from mountainous catchments during a global warming event, PETM, Southern Pyrenees, Spain. *Geophysical Research Letters*, *52*, e2024GL112404. https://doi.org/10.1029/2024GL112404

Received 10 SEP 2024
Accepted 5 MAR 2025

Author Contributions:

Conceptualization: M. Prieur, C. Robin, J. Braun, A. C. Whittaker, J. S. McLeod, C. Fillon, F. Schlunegger, T. O. Sømme, S. Castelltort
Formal analysis: M. Prieur
Funding acquisition: S. Castelltort
Methodology: M. Prieur, C. Robin, J. Braun, R. Jaimes-Gutierrez, A. Wild, L. Malatesta, S. Castelltort
Software: C. Robin, J. Braun
Supervision: J. Braun, A. C. Whittaker, C. Fillon, F. Schlunegger, T. O. Sømme, S. Castelltort
Validation: M. Prieur, J. Braun, S. Castelltort

1. Introduction

Sediment fluxes are fundamental metrics of Earth's surface dynamics and relate to erosion, transport, and deposition of clastic material. Changes in sediment flux can provide information on surface processes from source to sink and the effect of external forcings such as tectonics and climate (Allen et al., 2013; Peizhen et al., 2001; Romans et al., 2016; Tucker & Slingerland, 1997). Sediments are primarily generated in mountainous catchments from bedrock erosion via river incision, physical and chemical weathering, overland flow erosion, and landslides (Tucker & Slingerland, 1997; Tucker & Whipple, 2002). The resulting sediment flux from the source area impacts the volume of sediment eventually delivered to depositional sinks (Attal et al., 2015; Scherler et al., 2015; Tofelde et al., 2019).

Mountain catchments are the primary source of the sedimentary systems on which society relies, particularly floodplains and deltas (e.g., Viviroli et al., 2007). Global warming can lead to enhanced intensities of flood events and sediment transport due to wetter climate (Li et al., 2021). In the scope of current climate change, it is crucial to quantify the sensitivity of sediment generation and transport in a warming climate to predict the intensity and frequency of future catastrophic erosional events and floods to mitigate risks for the population (e.g., Lane et al., 2006). To that purpose, sedimentary archives and the estimation of paleo-sedimentary fluxes provide

Writing – original draft: M. Prieur
Writing – review & editing: C. Robin, J. Braun, R. Vaucher, A. C. Whittaker, R. Jaimes-Gutierrez, A. Wild, J. S. McLeod, L. Malatesta, C. Fillon, F. Schlunegger, T. O. Sømme, S. Castelltort

narratives of how Earth surface processes responded to past global warming (Pancost, 2017). The Paleocene-Eocene Thermal Maximum (PETM, ~56 Ma) was characterized by a rapid global rise in temperature of 3–8°C (Dunkley Jones et al., 2013; McInerney & Wing, 2011) over an onset phase of a few thousand years (e.g., Turner, 2018) causing major disruptions in hydroclimate by increasing seasonality and the occurrence of extreme floods (Carmichael et al., 2017; Rush et al., 2021). Moreover, the PETM caused a turnover of marine fauna (Alegret et al., 2009; Bowen et al., 2002) and a shift to sparser and less perennial vegetation (Schmitz et al., 2001; Wing et al., 2005).

Previous studies suggest that the PETM can be linked to enhanced global sediment fluxes (Carmichael et al., 2017; Sharman et al., 2023). This is hypothesized from increased depositional rates in shallow and deep-marine environments (e.g., Dunkley Jones et al., 2018; Giusberti et al., 2007; Jin et al., 2022; John et al., 2008; Schmitz et al., 2001; Self-Trail et al., 2012; Sharman et al., 2023; Sømme et al., 2023; Vimpere et al., 2023), and the progradation and lengthening of siliciclastic systems (Podrecca et al., 2021; Self-Trail et al., 2017; Sømme et al., 2023). These marine global observations correlate with enhanced erosion (John et al., 2012; Pogge von Strandmann et al., 2021) and weathering in the hinterlands (Dickson et al., 2014; Dickson et al., 2015; Khozyem et al., 2015; Pogge von Strandmann et al., 2021; Ramos et al., 2022; Ravizza et al., 2001; White & Schiebout, 2008), as well as enhanced channel mobility in the alluvial plains (Barefoot et al., 2021; Prieur, Whittaker, et al., 2024).

The hypothesis of a worldwide trend of increased sediment flux during the PETM generally relies on studies using one-dimensional well-log data instead of volume estimates (except Sømme et al., 2023). The issue is that 1D well-log data are inherently incomplete due to uneven deposition in time and space (Sadler, 1981; Straub & Esposito, 2013; Tipper, 1983, 2014). For a given time interval, the rock record results from successive depositional, stasis, and erosional events of unknown recurrence time and magnitude, reflecting different sedimentation variability (Barefoot et al., 2023; Paola et al., 2018; Straub et al., 2009; Tipper, 1983, 2014). Local one-dimensional estimates of sedimentation rates based on well data tend to be irregular over a sedimentary system (Sømme et al., 2023). Therefore, to capture all deposited and eroded sediments, we constrain volumes over a large depositional area and in a closed sedimentary basin, which improves the spatial stratigraphic completeness of the studied intervals (Aadland et al., 2018; Barefoot et al., 2023; Straub & Foreman, 2018) and allows a more reliable estimation of average sediment fluxes.

Although a large range of observations suggests that sediment flux and erosion increased with global warming during the PETM, the magnitude of this increase remains to be calculated from the rock record and across sedimentary basins. Quantifying sedimentary fluxes across the well-constrained PETM global warming is a unique opportunity to assess the sensitivity of sedimentary systems to climate. Here, we take advantage of temporally and geographically well-constrained sedimentary records covering fluvial and marine depozones of a small source-to-sink system. We compute sedimentary volumes before and during the climate crisis to reconstruct paleo-sedimentary fluxes and estimate how climate affected erosion. Then, we use two independent erosion models to test whether the variation in sediment flux can be explained by a scenario where sediments are produced by fluvial incision and associated overland flow erosion driven by changes in mean annual air temperature (MAAT) and mean annual precipitation (MAP) for the range of values suggested by three independent paleoclimate studies.

2. Study Area

2.1. The PETM in the South Pyrenean Foreland Basin

The PETM is well recorded in the stratigraphy of the South Pyrenean Foreland Basin (Spain). During the PETM, MAAT increased by 3–8°C in the Southern Pyrenees (Jaimes-Gutierrez et al., 2024; Khozyem, 2013; Rush et al., 2021). The models of Rush et al. (2021) suggest an increase in MAP and extreme event frequency and intensity. In marine deposits, increased terrigenous export during the PETM is inferred from a siliciclastic unit inserted between calcareous turbidites in Zumaia (Dunkley Jones et al., 2018) (Figure 1a), the sandstone infill of the Orio deep-sea channel (Pujalte et al., 2015) (Figure 1a), and delta progradation in the Ainsa Basin (Pujalte et al., 2016). Increased sediment flux during the PETM is also hypothesized from coarser sediments filling the Laminoria continental valley sourced from the Ebro Massif (Pujalte et al., 2015) (Figure 1a) and from the Claret Conglomerate in the Tremp Basin, sourced from the Pyrenees (Garcés et al., 2020; Gómez-Gras et al., 2016; Schmitz & Pujalte, 2007). The Claret Conglomerate corresponds to highly amalgamated conglomeratic fluvial

10.1029/2024GL112404

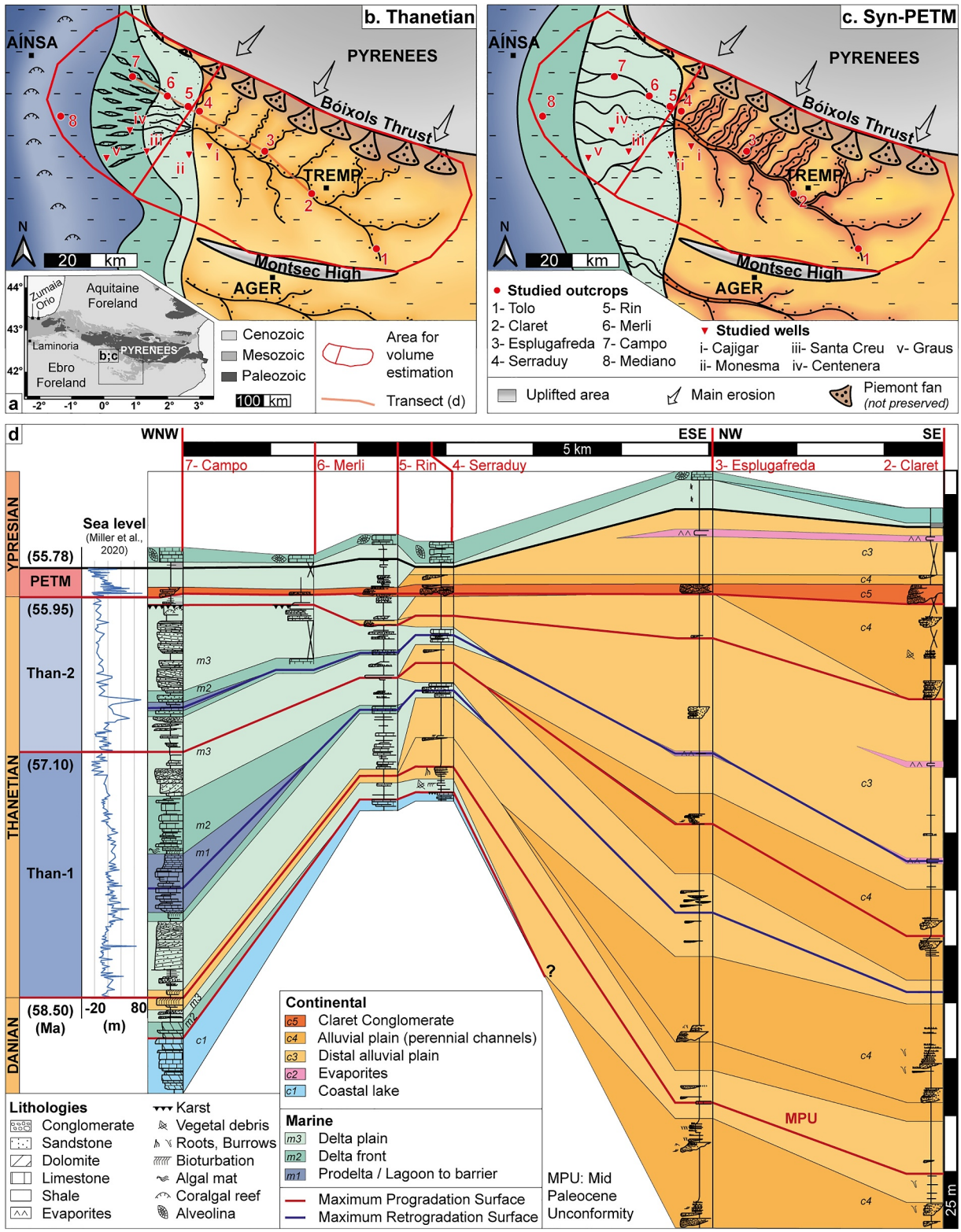

Figure 1. Study area. (a) Location map. (b) Paleogeography of the Tremp Basin during the Thanetian (modified from Gómez-Gras et al., 2016; Schmitz & Pujalte, 2007). (c) Paleogeography during the Paleocene-Eocene Thermal Maximum. (d) Correlation across the Tremp basin (Campo log modified from Eichenseer, 1988) (see all detailed sections in Supporting Information S1). Same color code as on paleogeographic maps (b, c). The sea-level curve from Miller et al. (2020) is interpolated linearly for each time interval.

channels deposited at the onset of the PETM and is interpreted as a braidplain widening (Schmitz & Pujalte, 2007) associated with increased water discharge (Chen et al., 2018) and enhanced channel mobility (Prieur, Whittaker, et al., 2024). Therefore, the coarsening of the siliciclastic facies and the overall system progradation trends hypothetically reflect an increase in sediment flux during the PETM in the Southern Pyrenees. However, no quantification to test this hypothesis has been carried out to-date.

2.2. The Tremp Basin: Sedimentary Fill of a Local Sink

The Tremp Basin developed as a piggyback between the Bóixols and Montsec thrusts (Beaumont et al., 2000) (Figures 1b and 1c). Its drainage area during the late Paleocene is restricted to the Pyrenees (Garcés et al., 2020; Mouthereau et al., 2014; Vacherat et al., 2017), and provenance studies indicate similar sources during the Early Eocene (Whitchurch et al., 2011), suggesting a constant drainage area across the PETM. To quantify sedimentary volumes, the Tremp Basin is a well-constrained example of a local sink located at the exit of the source catchment.

Tectonic features constrain the extent of the Tremp Basin. To the north, the Tremp Basin is bordered by the Bóixols Thrust. To the south, the topographic high induced by the Montsec Thrust formed a physical barrier that disconnected the Tremp Basin from the Ager Basin (Gómez-Gras et al., 2016) (Figures 1b and 1c). On the eastern side of the basin, provenance analyses carried out by Odlum et al. (2019) showed that the Tremp Basin is unlikely to have been connected to eastern sub-basins. Westward, the sedimentary system reached a marine embayment (Figures 1b and 1c): during the Thanetian, a bioclastic tide-dominated delta showed limited siliciclastic input from the hinterland (Eichenseer, 1988) (Figure 1b). At the end of the Thanetian, an incision phase induced a large valley network in the alluvial plain and the karstification of marine surfaces (Pujalte et al., 2014). After the filling of these valleys by the Incised Valley Fill member (IVF), the deposition of the Claret Conglomerate during the PETM records a lengthening of the siliciclastic system.

2.3. Time Constraints

The available chronostratigraphic constraints of the Paleocene to Lower Eocene infill of the Tremp Basin lead us to subdivide the record into three study intervals for estimating sediment volumes: (a) Thanetian-1 (Than-1), (b) Thanetian-2 (Than-2), and (c) the PETM (Figure 1). Than-1 starts at the top of the Mid-Paleocene Unconformity (Baceta et al., 2001, 2005, 2011), dated at 58.5 Ma based on biostratigraphic correlations (Baceta et al., 2001). The limit between Than-1 and Than-2 corresponds to the boundary between the NP8 and NP9 calcareous nannofossil zones (Baceta et al., 2005) coeval to the magnetozone C25n (Baceta et al., 2011; Raffi et al., 2016) dated at 57.1 ± 0.5 Ma (Westerhold et al., 2007). The age of the PETM initiation is 55.95 ± 0.05 Ma (Westerhold, Röhl, Donner, & Zachos, 2018; Zeebe & Lourens, 2019), and its duration is 170 ± 30 kyr (Abdul Aziz et al., 2008; Röhl et al., 2007; Westerhold, Röhl, Wilkens, et al., 2018; Zeebe & Lourens, 2019).

3. Materials and Methods

3.1. Area of Deposition and Sediment Thicknesses

To calculate a closed sedimentary budget with the aim of providing a complete sedimentary record, the studied area must encompass all the sediment exiting a catchment (Aadland et al., 2018; Barefoot et al., 2023; Straub & Foreman, 2018). For the Tremp Basin, the study area (red polygon in Figures 1b and 1c) is delimited by the Bóixols Thrust, Montsec High, and Montsec Thrust lateral ramp (see Section 2.2). The western limit of the study area, located west of Mediano, corresponds to the maximum extent of the bioclastic delta, with little siliciclastic input. Volume estimations do not include the Ainsa Basin, sourced by the Ebro Massif (Pujalte et al., 2016).

Sediment thicknesses are obtained from 8 outcrops and 5 wells (Figure 1; see detailed logs in the Supporting Information S1). These 13 sections, spanning terrestrial to marine depositional environments, allow the calculation of sedimentary volumes deposited along the entire sediment routing system. The limits between the three time-intervals defined in the literature correlate throughout the basin (Figure 1d; Supporting Information S1). The resulting one-dimensional thicknesses are implemented in the QGIS software and linearly interpolated within the study area to obtain the volume of sediments preserved in the basin per time interval.

3.2. Volume Calculation

Siliciclastic sedimentary volumes and their uncertainties are estimated over the Tremp Basin using the GIS-based method developed by Guillocheau et al. (2012), accounting for in-situ production, compaction, and porosity. In-situ production includes carbonate and evaporite precipitation and is calculated for each time interval (Supporting Information S1). In-situ production is significantly more important in marine carbonates. To reduce uncertainties, the study area is divided into two sub-areas: (a) an eastern area, mostly continental, and (b) a western area, mostly marine (Figures 1b and 1c).

3.3. The BQART Model

The BQART empirical model developed by Syvitski and Milliman (2007) from a large data set of modern erosional systems expresses the suspended sediment flux out of a catchment (Q_s) as a function of its lithology (l), soil erodibility (Eh), area (A), and relief (R), as well as the climate parameters: mean annual air temperature (MAAT) and mean annual water discharge. Mean annual water discharge is a function of the mean annual precipitation rate (MAP) and drainage area. As the temperatures were superior to 2°C in the PETM and given the absence of ice caps suggested by the warmhouse Paleocene climate (Westerhold et al., 2020), we apply the following equation (Syvitski & Milliman, 2007):

$$Q_s = \omega \,.\, l \,.\, Eh \,.\, \mathrm{MAP}^{0.31} \,.\, A^{0.81} \,.\, R \,.\, \mathrm{MAAT} \tag{1}$$

In Equation 1, ω equals 0.02 for Q_s expressed in $\mathrm{kg.s^{-1}}$ (Syvitski & Milliman, 2007). The lithology factor equals 2 for sedimentary rocks (Gómez-Gras et al., 2016; Nyberg et al., 2021; Syvitski & Milliman, 2007). The maximum Pyrenean relief is 0.9 ± 0.3 km based on thermochronology synthesis (Milesi et al., 2023). MAAT estimates are 24.5 ± 4.5°C for the Paleocene and 30.5 ± 3.5°C for the PETM (±1σ; Jaimes-Gutierrez et al., 2024; Khozyem, 2013; Rush et al., 2021), and MAP increases from 1.5 $\mathrm{m.yr^{-1}}$ to an average of 1.9 ± 0.5 $\mathrm{m.yr^{-1}}$ (±1σ) over the different climate models of Rush et al. (2021).

First, we calculate the drainage area from the inverted BQART equation using the Thanetian sediment fluxes obtained from field data. Then, we estimate the increase in sediment flux resulting from increases in MAP and MAAT in the range of values expected for the PETM. Finally, we test the sensitivity of Qs to wide ranges of increases in MAP (up to 15 $\mathrm{m.yr^{-1}}$), MAAT (up to 55°C), and Eh, the soil erosion parameter (up to 2). To estimate results' sensitivity to input parameters uncertainty, we performed Monte Carlo simulations with 10,000 runs (Nyberg et al., 2021; Zhang et al., 2018).

3.4. The Stream Power Law

The stream power law (SPL) expresses detachment-limited bedrock erosion (ε) in a catchment by a river as a function of its upstream drainage area (A), local slope (S), and erosion coefficient (K) (Howard et al., 1994; Whipple & Tucker, 1999).

$$\varepsilon = K \,.\, A^m \,.\, S^n \tag{2}$$

The exponents m and n relate to the dependence of erosion on water discharge and local slope, and they are commonly used with values of 0.5 and 1, respectively (Whipple & Tucker, 1999). Along the fluvial system, the drainage area is expressed as a power law of the distance to the divide (x) given two constant parameters (ka and h) (Hack, 1957). Moreover, the erosion coefficient is a function of precipitation rate (MAP) (Whipple & Tucker, 1999), leading to the following equation for the rate of change in elevation (dz/dt), expressed as a function of x for a given uplift rate (U):

$$\left(\frac{\partial z}{\partial t}\right)_t = U - K' \,.\, \mathrm{MAP}^m \,.\, \left(ka.x^h\right)^m \,.\, \left(\frac{\partial z}{\partial x}\right)^n \tag{3}$$

First, we initialize the model. The duration of the initialization, that is, the time needed to build the topography, is set such that the uplift and the altitude of the orogen meet Thanetian conditions. The range of K' values is determined such that, for a Thanetian MAP, the sedimentary flux out of the catchment reaches the Thanetian

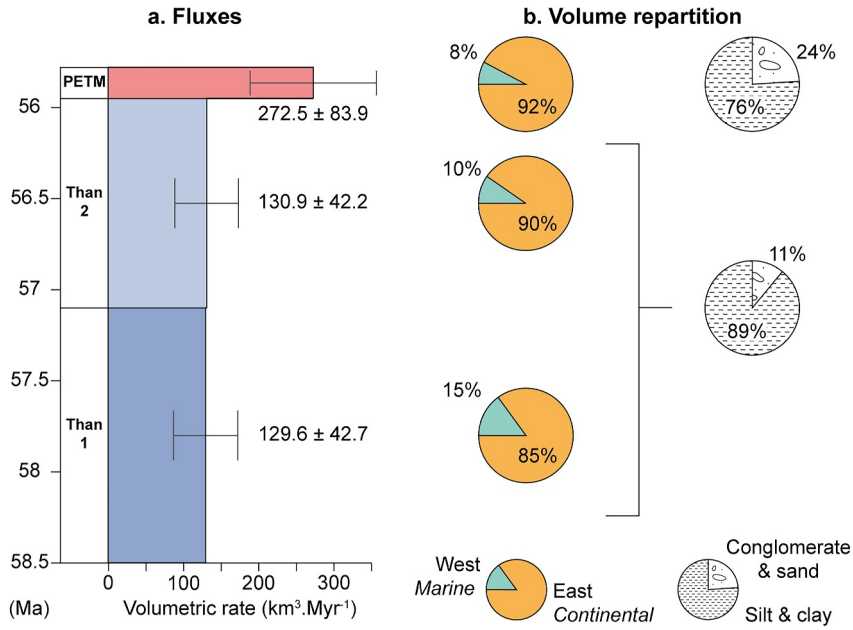

Figure 2. Sedimentary fluxes obtained from volume estimations. (a) Volumetric fluxes for each interval. The uncertainties are calculated after Guillocheau et al. (2012). (b) Repartition of the siliciclastic volumes in the eastern and western parts of the Tremp Basin for each period and ratios of conglomerate and sand lithologies versus silts and clays.

calculated values. With such values, note that the system is still transient. Following the initialization, we simulate a change in climatic conditions by imposing a step change in MAP over 200 kyrs. First, we calculate Qs corresponding to MAP in the range of PETM values. Then, we test the sensitivity of Qs to a wide range of MAP. The range of K' values is implemented in a Monte Carlo loop of 1,000 simulations. The model's output is the sediment flux at the exit of the catchment, which is then compared to field observations.

4. Results

4.1. Sedimentary Fluxes Across the PETM

The volumes of siliciclastic sediments deposited and preserved within the Tremp Basin are 181.4 ± 59.7 km^3 during Than-1, 150.5 ± 48.5 km^3 during Than-2, and 46.3 ± 14.3 km^3 during the PETM. According to the duration of these three periods (see Section 2.3), the sediment fluxes were 129.6 ± 42.7 $km^3.Myr^{-1}$ during Than-1, 130.9 ± 42.2 $km^3.Myr^{-1}$ during Than-2, and 272.5 ± 83.9 $km^3.Myr^{-1}$ during the PETM (Figure 2a). Therefore, Qs is constant during the Thanetian and increases by a factor of 2.1, on average, during the PETM global warming episode, the increase factor ranging from 1.1 to 4.

The subdivision between the eastern continental area and the western marine part of the basin suggests that continental deposits constitute 85%–92% of the sediment accumulation in the basin and decrease slightly with time (Figure 2b). Most of the siliciclastic volume comprises fine lithologies, with 89% made of silts and clays during the Thanetian and 76% during the PETM (Figure 2b).

4.2. Modeling

Using the BQART equation with Thanetian MAAT and MAP (Rush et al., 2021) and the calculated Thanetian Qs yields a median drainage area of 1,150 ± 600 km^2 for the Tremp Basin.

From the BQART model, the increases in MAAT and MAP (Rush et al., 2021) lead to a median sedimentary flux estimate of 168 $km^3.Myr^{-1}$ during the PETM, ranging from 119 $km^3.Myr^{-1}$ to 232 $km^3.Myr^{-1}$ at a 75% confidence interval (Figure 3a). Correcting the BQART suspension flux by a contribution of 20% bedload material, adequate for the considered drainage area (Hinderer et al., 2013) and the proportion of coarse sediments deposited in the basin (Figure 2b), results in a median PETM Qs of 202 $km^3.Myr^{-1}$, ranging from 143 $km^3.Myr^{-1}$ to

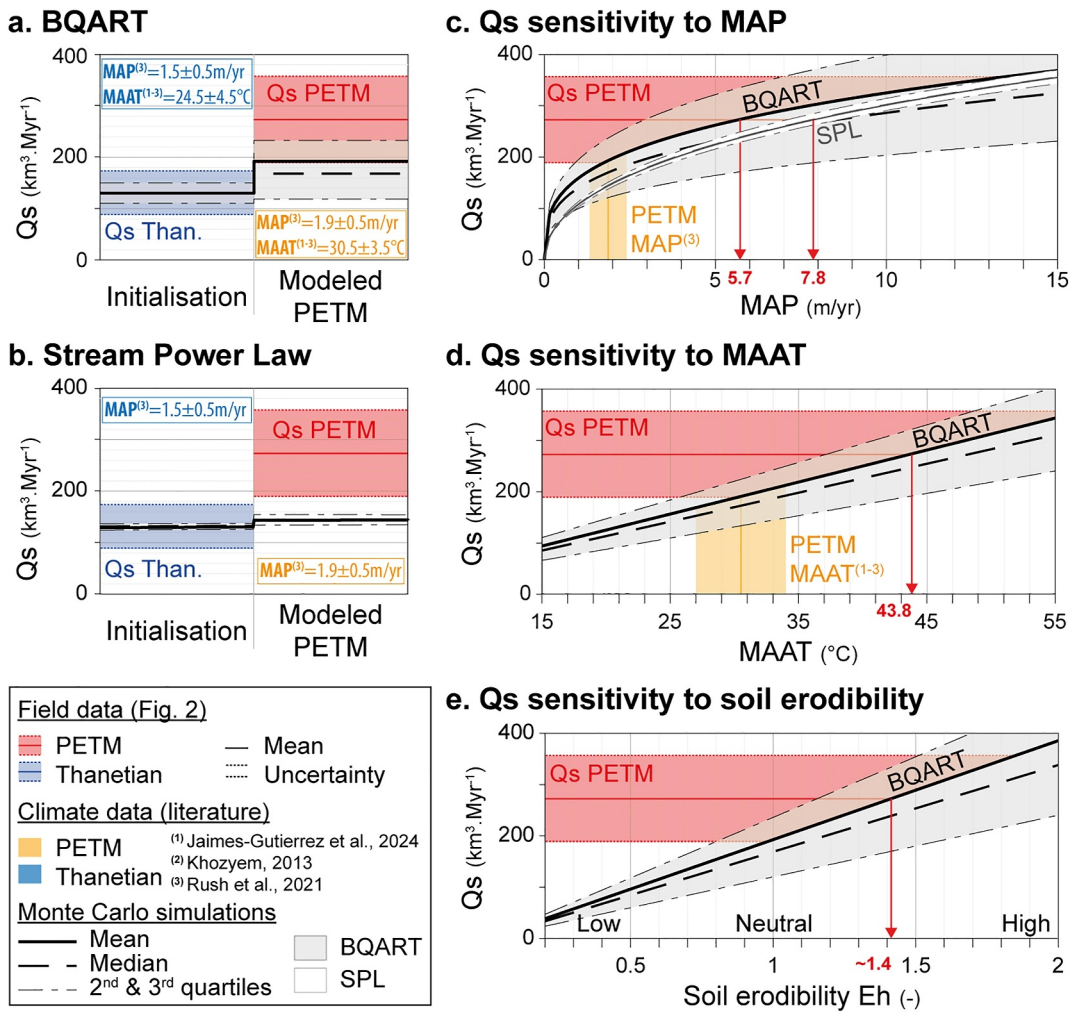

Figure 3. Model simulations compared to field results. (a) Qs simulated by the BQART equation. (b) Qs simulated by the stream power law (SPL). In panels (a, b), mean annual precipitation (MAP) and MAAT vary in the range of literature climate data. (c) Qs as a function of MAP from BQART and SPL. (d) Qs as a function of MAAT from BQART. (e) Qs as a function of soil erodibility from BQART. In panels (c, d, and e), red arrows indicate the MAP, MAAT, and Eh values that would be necessary to reach the calculated Paleocene-Eocene Thermal Maximum Qs.

278 $km^3.Myr^{-1}$. Changing MAP in the SPL leads to a sedimentary flux of 144 ± 10 $km^3.Myr^{-1}$ at 75% confidence interval during the PETM (Figure 3b). These estimates correspond to a multiplication of Qs by 1.1–1.6 from the Thanetian to the PETM, which fits within the lowest range of the values observed from the stratigraphy (Figure 2b).

However, to reach the average PETM fluxes, MAP values must reach 5.7 $m.yr^{-1}$ according to the BQART model and 7.8 $m.yr^{-1}$ according to the SPL simulation (Figure 3c). Fluxes from the BQART equation meet field values with a MAAT of 43.8°C (Figure 3d). These values are not realistic. Alternatively, Qs values in the range of the mean calculated for the PETM could be reached with an increase in soil erodibility by 40% (Figure 3e), which is more plausible given the change in vegetation from perennial during the Thanetian to seasonal during the PETM (Schmitz et al., 2001).

5. Discussion

5.1. Increase in Qs During the PETM Global Warming

Sediment flux is constant during the Thanetian at the time scale of the studied intervals, which is consistent with the absence of major changes in tectonics (Macchiavelli et al., 2017; Roest & Srivastava, 1991; Rosenbaum

et al., 2002) or climate (Westerhold et al., 2020) occurring during this period. Subsequently, sediment fluxes doubled during the PETM, which we hypothesize is not attributed to changes in drainage area, as detrital provenance in the Tremp Basin is similar from Paleocene to Early Eocene (Whitchurch et al., 2011). This two-fold increase is coherent with the conclusions drawn from the volumetric estimates of Qs in the Froan Basin (Norwegian Sea), where PETM fluxes are 2–4 times greater than pre-PETM and post-PETM fluxes (Sømme et al., 2023).

Nevertheless, we note each Thanetian interval spans 1.5 Myr, which is much longer than the 0.17 Myr duration of the PETM. Therefore, Qs variability for Than-1 and Than-2 over shorter timescales is averaged. In the context of uneven sedimentation, the possibility of missing high sedimentary flux events during the Thanetian is higher than during the PETM (Barefoot et al., 2023; Sadler, 1981; Straub et al., 2020; Straub & Foreman, 2018). However, the stratigraphic record of the syn-PETM Claret Conglomerate is unique as no other horizon is marked by such channel amalgamation and system progradation to the marine domain. Moreover, the Claret Conglomerate progradation occurs during a phase of sea-level rise (Figure 1d; Miller et al., 2020; Pujalte et al., 2014), which would have favored a retrogradation of the system, and it is unlikely to be driven by an autogenic advance of the system (Guerit et al., 2020) as it deposited over the interfluves of the Late Thanetian incised valleys (Pujalte et al., 2014). If a similar pulse in Qs had occurred during the Thanetian, we would expect it to be preserved in the stratigraphy (Straub & Esposito, 2013). Thus, it is unlikely that major Qs inputs are missed in our data during the Thanetian.

Sediment completeness is also altered by erosional stages (Barefoot et al., 2023; Sadler, 1981; Straub et al., 2020; Straub & Foreman, 2018). In the Tremp Basin, accounting for a mean thickness of 20 m for the late Paleocene incised valleys (Pujalte et al., 2014) and multiplying it by the entire continental area leads to a maximum estimate of the eroded volumes of about 40 km^3. This overestimation is smaller than the considered uncertainty. Although the IVF marks the only major erosional event described during the Thanetian in the Tremp Basin, the associated erosion had little effect on the trends observed in this study. Therefore, the incompleteness of the record falls within the uncertainties of the study.

The calculated volumes and Qs are minimum estimates due to (a) potential export toward the open ocean to the west and (b) underestimation of sediment thicknesses, especially at the footwall of the Bóixols Thrust, where subsidence was the highest. However, during the PETM, sediment export to the marine domain was enhanced (Dunkley Jones et al., 2018), subsidence was supposed to be constant (e.g., Macchiavelli et al., 2017), and sediment accumulation in alluvial fans likely increased due to enhanced Qs and subsequent increase in slope (Armitage et al., 2011). Therefore, PETM volumes are underestimated even more than the Thanetian ones, and the calculated increase in Qs is a lower bound.

5.2. Sensitivity of Erosion to Climate

The sedimentary volumes in the Tremp Basin recorded a doubling in Qs during the PETM. Coevally, paleoclimate studies suggest a MAAT increase of about 6 ± 2°C (±1σ) (Khozyem, 2013; Rush et al., 2021), and a 27 ± 33% (±1σ) rise in MAP (Rush et al., 2021). Yet, implementing these MAP and MAAT estimates in the BQART and the SPL explains only 9%–27% of the increase in Qs calculated from sedimentary volumes. This is because the BQART and SPL express Qs as a function of MAP to the power of 0.31 and 0.5, respectively. According to these equations, doubling Qs would require a quadrupling or more in MAP. Even if larger values were used for m and n in the SPL (e.g., Lague, 2014), using $m = 1$ would still require a doubling of MAP to double Qs. Therefore, even though paleoclimate reconstructions bear uncertainties (e.g., Lunt et al., 2013), the MAP and MAAT values that would be needed to explain the rise in Qs according to the BQART and SPL are unrealistically too high (Rush et al., 2021).

5.3. Sedimentary Processes in a Warming World

Climate models also suggest enhanced intensity of extreme rainfall events during the PETM in the Southern Pyrenees (Rush et al., 2021). Therefore, processes of sediment generation were likely not limited to bedrock fluvial incision and overland flow erosion controlled by mean annual climate conditions, as modeled by the BQART and SPL. The "system-clearing" event scenario (Jerolmack & Paola, 2010) could explain the abrupt progradation of coarse materials down-system once a threshold is reached, as demonstrated by Armitage et al. (2011) and observed during the PETM in the Tremp Basin (Chen et al., 2018; Duller et al., 2019) and other

basins in the USA (Barefoot et al., 2021; Foreman, 2014; Foreman et al., 2012), and in Peru (Schlunegger et al., 2023). Under this hypothesis, dramatic sediment evacuation from the source area would have propagated along the sedimentary system driven by landslides (Hovius et al., 1997), floods (Baynes et al., 2015; McLeod et al., 2024), and floodplain reworking (Prieur, Whittaker, et al., 2024).

The trigger for exceeding the erosion threshold may be due to the significantly warmer temperatures during the hothouse PETM (Westerhold et al., 2020), linked to a higher frequency of extreme rainfall events (Coumou & Rahmstorf, 2012; Domeisen & Butler, 2020) and enhanced landslides (Gariano & Guzzetti, 2016) leading to increased sediment fluxes (Cecil & Dulong, 2003; Molnar, 2001). The discrepancy between this study's field and model results shows that more complex erosional processes were at play during the PETM global warming, also likely influenced by wildfires and vegetation changes (Denis et al., 2017). Further studies are needed to test if increased rainfall variability during the PETM (Carmichael et al., 2017; Rush et al., 2021) would explain the observed rise in Qs.

6. Conclusions

We quantify the impact of a past climate perturbation on erosion and sediment flux. During the PETM in the southern Pyrenees, we document an average 2-fold increase in sediment fluxes compared to that generated for the previous 2.6 Myr. According to paleoclimate studies, this doubling in Qs concomitates with a 3–8°C increase in MAAT and a 27% increase in MAP. However, BQART and SPL erosion models indicate that such changes in MAP and MAAT seem insufficient to generate the change in documented sediment volumes. These results suggest that river incision driven just by mean annual climate parameters cannot adequately explain variations in Qs during a sudden climate warming event. Instead, we hypothesize that changes in seasonality likely played a key role in the erosion and transport of sediments. In today's warming world, this study suggests that climate averages are likely to underpredict the erosional impact of environmental change, and we argue that further studies constraining the impact of seasonality and climate extremes are urgently needed to reconcile PETM sediment budgets effectively.

Data Availability Statement

The Matlab code used for the BQART and stream power law models is available from Zenodo (Prieur, Robin, et al., 2024).

Acknowledgments
This project has been funded by the European Union's H2020 program (Marie Sklodowska-Curie Grant 860383). We thank Robert Duller and two anonymous reviewers for constructive comments.

References

Aadland, T., Sadler, P. M., & Helland-Hansen, W. (2018). Geometric interpretation of time-scale dependent sedimentation rates. *Sedimentary Geology*, *371*, 32–40. https://doi.org/10.1016/j.sedgeo.2018.04.003

Abdul Aziz, H., Hilgen, F. J., van Luijk, G. M., Sluijs, A., Kraus, M. J., Pares, J. M., & Gingerich, P. D. (2008). Astronomical climate control on paleosol stacking patterns in the upper Paleocene–lower Eocene Willwood Formation, Bighorn Basin, Wyoming. *Geology*, *36*(7), 531. https://doi.org/10.1130/g24734a.1

Alegret, L., Ortiz, S., Orue-Etxebarria, X., Bernaola, G., Baceta, J. I., Monechi, S., et al. (2009). The paleocene-eocene thermal maximum: New data on microfossil turnover at the Zumaia section, Spain. *PALAIOS*, *24*(5), 318–328. https://doi.org/10.2110/palo.2008.p08-057r

Allen, P. A., Armitage, J. J., Carter, A., Duller, R. A., Michael, N. A., Sinclair, H. D., et al. (2013). The Qs problem: Sediment volumetric balance of proximal foreland basin systems. *Sedimentology*, *60*(1), 102–130. https://doi.org/10.1111/sed.12015

Armitage, J. J., Duller, R. A., Whittaker, A. C., & Allen, P. A. (2011). Transformation of tectonic and climatic signals from source to sedimentary archive. *Nature Geoscience*, *4*(4), 231–235. https://doi.org/10.1038/ngeo1087

Attal, M., Mudd, S. M., Hurst, M. D., Weinman, B., Yoo, K., & Naylor, M. (2015). Impact of change in erosion rate and landscape steepness on hillslope and fluvial sediments grain size in the Feather River basin (Sierra Nevada, California). *Earth Surface Dynamics*, *3*(1), 201–222. https://doi.org/10.5194/esurf-3-201-2015

Baceta, J. I., Pujalte, V., & Bernaola, G. (2005). Paleocene coralgal reefs of the western Pyrenean basin, northern Spain: New evidence supporting an earliest Paleogene recovery of reefal ecosystems. *Palaeogeography, Palaeoclimatology, Palaeoecology*, *224*(1–3), 117–143. https://doi.org/10.1016/j.palaeo.2005.03.033

Baceta, J. I., Pujalte, V., Wright, V. P., & Schmitz, B. (2011). Carbonate platform models, sea/level changes and extreme climatic events during the Paleocene/early Eocene greenhouse interval: A basinbasin-platform-coastal plain transect across the southern Pyrenean basin. Paper presented at the 28th IAS Meeting of Sedimentology, Zaragoza.

Baceta, J. I., Wright, V. P., & Pujalte, V. (2001). Paleo-mixing zone karst features from Palaeocene carbonates of north Spain: Criteria for recognizing a potentially widespread but rarely documented diagenetic system. *Sedimentary Geology*, *139*(3–4), 205–216. https://doi.org/10.1016/s0037-0738(00)00166-4

Barefoot, E. A., Nittrouer, J. A., Foreman, B. Z., Hajek, E. A., Dickens, G. R., Baisden, T., & Toms, L. (2021). Evidence for enhanced fluvial channel mobility and fine sediment export due to precipitation seasonality during the Paleocene-Eocene thermal maximum. *Geology*, *50*(1), 116–120. https://doi.org/10.1130/g49149.1

Barefoot, E. A., Nittrouer, J. A., & Straub, K. M. (2023). Sedimentary processes and the temporal resolution of sedimentary Strata. *Geophysical Research Letters*, *50*(13). https://doi.org/10.1029/2023gl103925

Baynes, E. R. C., Attal, M., Niedermann, S., Kirstein, L. A., Dugmore, A. J., & Naylor, M. (2015). Erosion during extreme flood events dominates Holocene canyon evolution in northeast Iceland. *Proceedings of the National Academy of Sciences*, *112*(8), 2355–2360. https://doi.org/10.1073/pnas.1415443112

Beaumont, C., Muñoz, J. A., Hamilton, J., & Fullsack, P. (2000). Factors controlling the Alpine evolution of the central Pyrenees inferred from a comparison of observations and geodynamical models. *Journal of Geophysical Research*, *105*(B4), 8121–8145. https://doi.org/10.1029/1999jb900390

Bowen, G. J., Clyde, W. C., Koch, P. L., Ting, S., Alroy, J., Tsubamoto, T., et al. (2002). Mammalian dispersal at the Paleocene/Eocene boundary. *Science*, *295*(5562), 2062–2065. https://doi.org/10.1126/science.1068700

Carmichael, M. J., Inglis, G. N., Badger, M. P. S., Naafs, B. D. A., Behrooz, L., Remmelzwaal, S., et al. (2017). Hydrological and associated biogeochemical consequences of rapid global warming during the Paleocene-Eocene Thermal Maximum. *Global and Planetary Change*, *157*, 114–138. https://doi.org/10.1016/j.gloplacha.2017.07.014

Cecil, C. B., & Dulong, F. T. (2003). Precipitation models for sediment supply in warm climates. In C. B. Cecil & N. T. Edgar (Eds.), *Climate controls on stratigraphy* (Vol. 77, pp. 21–27). SEPM Society for Sedimentary Geology. https://doi.org/10.2110/pec.03.77.0021

Chen, C., Guerit, L., Foreman, B. Z., Hassenruck-Gudipati, H. J., Adatte, T., Honegger, L., et al. (2018). Estimating regional flood discharge during Palaeocene-Eocene global warming. *Scientific Reports*, *8*(1), 13391. https://doi.org/10.1038/s41598-018-31076-3

Coumou, D., & Rahmstorf, S. (2012). A decade of weather extremes. *Nature Climate Change*, *2*(7), 491–496. https://doi.org/10.1038/nclimate1452

Denis, E. H., Pedentchouk, N., Schouten, S., Pagani, M., & Freeman, K. H. (2017). Fire and ecosystem change in the Arctic across the Paleocene–Eocene thermal maximum. *Earth and Planetary Science Letters*, *467*, 149–156. https://doi.org/10.1016/j.epsl.2017.03.021

Dickson, A. J., Cohen, A. S., Coe, A. L., Davies, M., Shcherbinina, E. A., & Gavrilov, Y. O. (2015). Evidence for weathering and volcanism during the PETM from Arctic Ocean and Peri-Tethys osmium isotope records. *Palaeogeography, Palaeoclimatology, Palaeoecology*, *438*, 300–307. https://doi.org/10.1016/j.palaeo.2015.08.019

Dickson, A. J., Rees-Owen, R. L., März, C., Coe, A. L., Cohen, A. S., Pancost, R. D., et al. (2014). The spread of marine anoxia on the northern Tethys margin during the Paleocene-Eocene Thermal Maximum. *Paleoceanography*, *29*(6), 471–488. https://doi.org/10.1002/2014pa002629

Domeisen, D. I. V., & Butler, A. H. (2020). Stratospheric drivers of extreme events at the Earth's surface. *Communications Earth & Environment*, *1*(1), 59. https://doi.org/10.1038/s43247-020-00060-z

Duller, R. A., Armitage, J. J., Manners, H. R., Grimes, S., & Jones, T. D. (2019). Delayed sedimentary response to abrupt climate change at the Paleocene-Eocene boundary, northern Spain. *Geology*, *47*(2), 159–162. https://doi.org/10.1130/g45631.1

Dunkley Jones, T., Lunt, D. J., Schmidt, D. N., Ridgwell, A., Sluijs, A., Valdes, P. J., & Maslin, M. (2013). Climate model and proxy data constraints on ocean warming across the Paleocene–Eocene Thermal Maximum. *Earth-Science Reviews*, *125*, 123–145. https://doi.org/10.1016/j.earscirev.2013.07.004

Dunkley Jones, T., Manners, H. R., Hoggett, M., Kirtland Turner, S., Westerhold, T., Leng, M. J., et al. (2018). Dynamics of sediment flux to a bathyal continental margin section through the Paleocene–Eocene Thermal Maximum. *Climate of the Past*, *14*(7), 1035–1049. https://doi.org/10.5194/cp-14-1035-2018

Eichenseer, H. (1988). Facies geology of late Maastrichtian to early Eocene coastal and shallow marine sediments (Tremp-Graus Basin, northeastern Spain). (PhD).

Foreman, B. Z. (2014). Climate-driven generation of a fluvial sheet sand body at the Paleocene–Eocene boundary in north-west Wyoming (USA). *Basin Research*, *26*(2), 225–241. https://doi.org/10.1111/bre.12027

Foreman, B. Z., Heller, P. L., & Clementz, M. T. (2012). Fluvial response to abrupt global warming at the Palaeocene/Eocene boundary. *Nature*, *491*(7422), 92–95. https://doi.org/10.1038/nature11513

Garcés, M., López-Blanco, M., Valero, L., Beamud, E., Muñoz, J. A., Oliva-Urcia, B., et al. (2020). Paleogeographic and sedimentary evolution of the South Pyrenean foreland basin. *Marine and Petroleum Geology*, *113*, 104105.

Gariano, S. L., & Guzzetti, F. (2016). Landslides in a changing climate. *Earth-Science Reviews*, *162*, 227–252. https://doi.org/10.1016/j.earscirev.2016.08.011

Giusberti, L., Rio, D., Agnini, C., Backman, J., Fornaciari, E., Tateo, F., & Oddone, M. (2007). Mode and tempo of the Paleocene-Eocene thermal maximum in an expanded section from the Venetian pre-Alps. *Geological Society of America Bulletin*, *119*(3–4), 391–412. https://doi.org/10.1130/b25994.1

Gómez-Gras, D., Roigé, M., Fondevilla, V., Oms, O., Boya, S., & Remacha, E. (2016). Provenance constraints on the Tremp formation paleogeography (southern Pyrenees): Ebro Massif VS Pyrenees sources. *Cretaceous Research*, *57*, 414–427. https://doi.org/10.1016/j.cretres.2015.09.010

Guerit, L., Foreman, B. Z., Chen, C., Paola, C., & Castelltort, S. (2020). Autogenic delta progradation during sea-level rise within incised valleys. *Geology*, *49*(3), 273–277. https://doi.org/10.1130/g47976.1

Guillocheau, F., Rouby, D., Robin, C., Helm, C., Rolland, N., Le Carlier de Veslud, C., & Braun, J. (2012). Quantification and causes of the terrigeneous sediment budget at the scale of a continental margin: A new method applied to the Namibia–South Africa margin. *Basin Research*, *24*(1), 3–30. https://doi.org/10.1111/j.1365-2117.2011.00511.x

Hack, J. T. (1957). *Studies of longitudinal stream profiles in Virginia and Maryland*. USGS.

Hinderer, M., Kastowski, M., Kamelger, A., Bartolini, C., & Schlunegger, F. (2013). River loads and modern denudation of the Alps—A review. *Earth-Science Reviews*, *118*, 11–44.

Hovius, N., Stark, C. P., & Allen, P. A. (1997). Sediment flux from a mountain belt derived by landslide mapping. *Geology*, *25*(3), 231–234. https://doi.org/10.1130/0091-7613(1997)025<0231:sffamb>2.3.co;2

Howard, A. D., Dietrich, W. E., & Seidl, M. A. (1994). Modeling fluvial erosion on regional to continental scales. *Journal of Geophysical Research*, *99*(B7), 13971–13986. https://doi.org/10.1029/94jb00744

Jaimes-Gutierrez, R., Adatte, T., Pucéat, E., Vennemann, T., Prieur, M., Wild, A., et al. (2024). Deciphering Paleocene-Eocene thermal maximum climatic dynamics: Insights from oxygen and hydrogen isotopes in clay minerals of paleosols from the southern Pyrenees. *Paleoceanography and Paleoclimatology*, *39*(11). https://doi.org/10.1029/2024pa004858

Jerolmack, D. J., & Paola, C. (2010). Shredding of environmental signals by sediment transport. *Geophysical Research Letters*, *37*(19). https://doi.org/10.1029/2010gl044638

Jin, S., Kemp, D. B., Jolley, D. W., Vieira, M., Zachos, J. C., Huang, C., et al. (2022). Large-scale, astronomically paced sediment input to the north sea Basin during the Paleocene Eocene thermal maximum. *Earth and Planetary Science Letters*, *579*, 117340. https://doi.org/10.1016/j.epsl.2021.117340

John, C. M., Banerjee, N. R., Longstaffe, F. J., Sica, C., Law, K. R., & Zachos, J. C. (2012). Clay assemblage and oxygen isotopic constraints on the weathering response to the Paleocene-Eocene thermal maximum, east coast of North America. *Geology*, *40*(7), 591–594. https://doi.org/10.1130/g32785.1

John, C. M., Bohaty, S. M., Zachos, J. C., Sluijs, A., Gibbs, S., Brinkhuis, H., & Bralower, T. J. (2008). North American continental margin records of the Paleocene-Eocene thermal maximum: Implications for global carbon and hydrological cycling. *Paleoceanography*, *23*(2). https://doi.org/10.1029/2007pa001465

Khozyem, H. (2013). Sedimentology, geochemistry and mineralogy of the Paleocene-Eocene thermal maximum (PETM): Sediment records from Egypt, India and Spain. (PhD).

Khozyem, H., Adatte, T., Spangenberg, J. E., Keller, G., Tantawy, A. A., & Ulianov, A. (2015). New geochemical constraints on the Paleocene–Eocene thermal maximum: Dababiya GSSP, Egypt. *Palaeogeography, Palaeoclimatology, Palaeoecology*, *429*, 117–135. https://doi.org/10.1016/j.palaeo.2015.04.003

Lague, D. (2014). The stream power river incision model: Evidence, theory and beyond. *Earth Surface Processes and Landforms*, *39*(1), 38–61. https://doi.org/10.1002/esp.3462

Lane, S. N., Tayefi, V., Reid, S. C., Yu, D., & Hardy, R. J. (2006). Interactions between sediment delivery, channel change, climate change and flood risk in a temperate upland environment. *Earth Surface Processes and Landforms*, *32*(3), 429–446. https://doi.org/10.1002/esp.1404

Li, D., Lu, X., Overeem, I., Walling, D. E., Syvitski, J., Kettner, A. J., et al. (2021). Exceptional increases in fluvial sediment fluxes in a warmer and wetter High Mountain Asia. *Science*, *374*(6567), 599–603. https://doi.org/10.1126/science.abi9649

Lunt, D. J., Elderfield, H., Pancost, R., Ridgwell, A., Foster, G. L., Haywood, A., et al. (2013). Warm climates of the past—A lesson for the future? *Philosophical Transactions of the Royal Society A: Mathematical, Physical & Engineering Sciences*, *371*(2001), 20130146.

Macchiavelli, C., Vergés, J., Schettino, A., Fernàndez, M., Turco, E., Casciello, E., et al. (2017). A new southern North Atlantic Isochron map: Insights into the Drift of the Iberian plate since the late Cretaceous. *Journal of Geophysical Research: Solid Earth*, *122*(12), 9603–9626. https://doi.org/10.1002/2017jb014769

McInerney, F. A., & Wing, S. L. (2011). The Paleocene-Eocene thermal maximum: A perturbation of carbon cycle, climate, and biosphere with implications for the future. *Annual Review of Earth and Planetary Sciences*, *39*(1), 489–516. https://doi.org/10.1146/annurev-earth-040610-133431

McLeod, J. S., Whittaker, A. C., Bell, R. E., Hampson, G. J., Watkins, S. E., Brooke, S. A. S., et al. (2024). Landscapes on the edge: River intermittency in a warming world. *Geology*, *52*(7), 512–516. https://doi.org/10.1130/g52043.1

Milesi, G., Valla, P. G., Münch, P., & Huyghe, D. (2023). Tectono-geomorphological evolution of the eastern Pyrenees: Insights from thermo-kinematic modeling. *Tectonophysics*, *866*, 230057. https://doi.org/10.1016/j.tecto.2023.230057

Miller, K. G., Schmelz, W. J., Browning, J. V., Kopp, R. E., Mountain, G. S., & Wright, J. D. (2020). Ancient sea level as key to the future. *Paleoceanography*, *33*(2). https://doi.org/10.5670/oceanog.2020.224

Molnar, P. (2001). Climate change, flooding in arid environments, and erosion rates. *Geology*, *29*(12), 1071–1074. https://doi.org/10.1130/0091-7613(2001)029<1071:ccfiae>2.0.co;2

Mouthereau, F., Filleaudeau, P.-Y., Vacherat, A., Pik, R., Lacombe, O., Fellin, M. G., et al. (2014). Placing limits to shortening evolution in the Pyrenees: Role of margin architecture and implications for the Iberia/Europe convergence. *Tectonics*, *33*(12), 2283–2314. https://doi.org/10.1002/2014tc003663

Nyberg, B., Helland-Hansen, W., Gawthorpe, R., Tillmans, F., & Sandbakken, P. (2021). Assessing first-order BQART estimates for ancient source-to-sink mass budget calculations. *Basin Research*, *33*(4), 2435–2452. https://doi.org/10.1111/bre.12563

Odlum, M. L., Stockli, D. F., Capaldi, T. N., Thomson, K. D., Clark, J., Puigdefàbregas, C., & Fildani, A. (2019). Tectonic and sediment provenance evolution of the South Eastern Pyrenean foreland basins during rift margin inversion and orogenic uplift. *Tectonophysics*, *765*, 226–248. https://doi.org/10.1016/j.tecto.2019.05.008

Pancost, R. D. (2017). Climate change narratives. *Nature Geoscience*, *10*(7), 466–468. https://doi.org/10.1038/ngeo2981

Paola, C., Ganti, V., Mohrig, D., Runkel, A. C., & Straub, K. M. (2018). Time not our time: Physical controls on the preservation and measurement of geologic time. *Annual Review of Earth and Planetary Sciences*, *46*(46), 409–438. https://doi.org/10.1146/annurev-earth-082517-010129

Peizhen, Z., Molnar, P., & Downs, W. R. (2001). Increased sedimentation rates and grain sizes 2-4 Myr ago due to the influence of climate change on erosion rates. *Nature*, *410*(6831), 891–897. https://doi.org/10.1038/35073504

Podrecca, L. G., Makarova, M., Miller, K. G., Browning, J. V., & Wright, J. D. (2021). Clear as mud: Clinoform progradation and expanded records of the Paleocene-Eocene thermal maximum. *Geology*, *49*(12), 1441–1445. https://doi.org/10.1130/g49061.1

Pogge von Strandmann, P. A. E., Jones, M. T., West, A. J., Murphy, M. J., Stokke, E. W., Tarbuck, G., et al. (2021). Lithium isotope evidence for enhanced weathering and erosion during the Paleocene-Eocene Thermal Maximum. *Science Advances*, *7*(42). https://doi.org/10.1126/sciadv.abh4224

Prieur, M., Robin, C., Braun, J., Vaucher, R., Whittaker, A. C., Jaimes-Gutierrez, R., et al. (2024). [Data Repository] Matlab Script for BQART and stream power law Modeling of the Impact of PETM on sediment flux. In *The southern Pyrenees (Tremp Basin)*. https://doi.org/10.5281/zenodo.13692043

Prieur, M., Whittaker, A. C., Nuriel, P., Jaimes-Gutierrez, R., Garzanti, E., Roigé, M., et al. (2024). Fingerprinting enhanced floodplain reworking during the Paleocene−Eocene thermal maximum in the southern Pyrenees (Spain): Implications for channel dynamics and carbon burial. *Geology*, *52*(9), 651–655. https://doi.org/10.1130/G52180.1

Pujalte, V., Baceta, J. I., & Schmitz, B. (2015). A massive input of coarse-grained siliciclastics in the Pyrenean Basin during the PETM: The missing ingredient in a coeval abrupt change in hydrological regime. *Climate of the Past*, *11*(12), 1653–1672. https://doi.org/10.5194/cp-11-1653-2015

Pujalte, V., Robador, A., Payros, A., & Samsó, J. M. (2016). A siliciclastic braid delta within a lower Paleogene carbonate platform (Ordesa-Monte Perdido National Park, southern Pyrenees, Spain): Record of the Paleocene–Eocene thermal maximum perturbation. *Palaeogeography, Palaeoclimatology, Palaeoecology*, *459*, 453–470. https://doi.org/10.1016/j.palaeo.2016.07.029

Pujalte, V., Schmitz, B., & Baceta, J. I. (2014). Sea-level changes across the Paleocene–Eocene interval in the Spanish Pyrenees, and their possible relationship with North Atlantic magmatism. *Palaeogeography, Palaeoclimatology, Palaeoecology*, *393*, 45–60. https://doi.org/10.1016/j.palaeo.2013.10.016

Raffi, I., Agnini, C., Backman, J., Catanzariti, R., & Pälike, H. (2016). A Cenozoic calcareous nannofossil biozonation from low and middle latitudes: A synthesis. *Journal of Nannoplankton Research*, *36*(2), 121–132. https://doi.org/10.58998/jnr2206

Ramos, E. J., Breecker, D. O., Barnes, J. D., Li, F., Gingerich, P. D., Loewy, S. L., et al. (2022). Swift weathering response on floodplains during the Paleocene-Eocene thermal maximum. *Geophysical Research Letters*, *49*(6). https://doi.org/10.1029/2021gl097436

Ravizza, G., Norris, R. N., Blusztajn, J., & Aubry, M. P. (2001). An osmium isotope excursion associated with the Late Paleocene thermal maximum: Evidence of intensified chemical weathering. *Paleoceanography*, *16*(2), 155–163. https://doi.org/10.1029/2000pa000541

Roest, W. R., & Srivastava, S. P. (1991). Kinematics of the plate boundaries between Eurasia, Iberia, and Africa in the north Atlantic from the late Cretaceous to the present. *Geology*, *19*(6), 613–616. https://doi.org/10.1130/0091-7613(1991)019<0613:kotpbb>2.3.co;2

Röhl, U., Westerhold, T., Bralower, T. J., & Zachos, J. C. (2007). On the duration of the Paleocene-Eocene thermal maximum (PETM). *Geochemistry, Geophysics, Geosystems*, *8*(12). https://doi.org/10.1029/2007gc001784

Romans, B. W., Castelltort, S., Covault, J. A., Fildani, A., & Walsh, J. P. (2016). Environmental signal propagation in sedimentary systems across timescales. *Earth-Science Reviews*, *153*, 7–29. https://doi.org/10.1016/j.earscirev.2015.07.012

Rosenbaum, G., Lister, G. S., & Duboz, C. (2002). Relative motions of Africa, Iberia and Europe during the Alpine orogeny. *Tectonophysics*, *359*(1–2), 117–129. https://doi.org/10.1016/s0040-1951(02)00442-0

Rush, W. D., Kiehl, J. T., Shields, C. A., & Zachos, J. C. (2021). Increased frequency of extreme precipitation events in the North Atlantic during the PETM: Observations and theory. *Palaeogeography, Palaeoclimatology, Palaeoecology*, *568*, 110289. https://doi.org/10.1016/j.palaeo.2021.110289

Sadler, P. M. (1981). Sediment accumulation rates and the completeness of stratigraphic sections. *The Journal of Geology*, *89*(5), 569–584. https://doi.org/10.1086/628623

Scherler, D., Bookhagen, B., Wulf, H., Preusser, F., & Strecker, M. R. (2015). Increased late Pleistocene erosion rates during fluvial aggradation in the Garhwal Himalaya, northern India. *Earth and Planetary Science Letters*, *428*, 255–266. https://doi.org/10.1016/j.epsl.2015.06.034

Schlunegger, F., do Prado, A. H., Norton, K. P., & Delunel, R. (2023). On the mechanisms resulting in the formation of the Quaternary staircase terrace systems in the valleys of the western Andean margin of Peru. *Geomorphology*, *442*, 108923. https://doi.org/10.1016/j.geomorph.2023.108923

Schmitz, B., & Pujalte, V. (2007). Abrupt increase in seasonal extreme precipitation at the Paleocene-Eocene boundary. *Geology*, *35*(3), 215. https://doi.org/10.1130/g23261a.1

Schmitz, B., Pujalte, V., & Núñez-Betelu, K. (2001). Climate and sea-level perturbations during the initial Eocene thermal maximum: Evidence from siliciclastic units in the Basque basin (Ermua, Zumaia and Trabakua Pass), northern Spain. *Palaeogeography, Palaeoclimatology, Palaeoecology*, *165*(3–4), 299–320.

Self-Trail, J. M., Powars, D. S., Watkins, D. K., & Wandless, G. A. (2012). Calcareous nannofossil assemblage changes across the Paleocene–Eocene thermal maximum: Evidence from a shelf setting. *Marine Micropaleontology*, *92–93*, 61–80. https://doi.org/10.1016/j.marmicro.2012.05.003

Self-Trail, J. M., Robinson, M. M., Bralower, T. J., Sessa, J. A., Hajek, E. A., Kump, L. R., et al. (2017). Shallow marine response to global climate change during the Paleocene-Eocene thermal maximum, Salisbury embayment, USA. *Paleoceanography*, *32*(7), 710–728. https://doi.org/10.1002/2017pa003096

Sharman, G. R., Szymanski, E., Hackworth, R. A., Kahn, A. C. M., Febo, L. A., Oefinger, J., & Gregory, G. M. (2023). Carbon isotope chemostratigraphy, geochemistry, and biostratigraphy of the Paleocene–Eocene thermal maximum, deepwater Wilcox Group, Gulf of Mexico (USA). *Climate of the Past*, *19*(9), 1743–1775. https://doi.org/10.5194/cp-19-1743-2023

Sømme, T. O., Huwe, S. I., Martinsen, O. J., Sandbakken, P. T., Skogseid, J., & Valore, L. A. (2023). Stratigraphic expression of the Paleocene-Eocene thermal maximum climate event during long-lived transient uplift—An example from a shallow to deep-marine clastic system in the Norwegian sea. *Frontiers in Earth Science*, *11*. https://doi.org/10.3389/feart.2023.1082203

Straub, K. M., Duller, R. A., Foreman, B. Z., & Hajek, E. A. (2020). Buffered, incomplete, and Shredded: The challenges of reading an imperfect stratigraphic record. *Journal of Geophysical Research: Earth Surface*, *125*(3). https://doi.org/10.1029/2019jf005079

Straub, K. M., & Esposito, C. R. (2013). Influence of water and sediment supply on the stratigraphic record of alluvial fans and deltas: Process controls on stratigraphic completeness. *Journal of Geophysical Research: Earth Surface*, *118*(2), 625–637. https://doi.org/10.1002/jgrf.20061

Straub, K. M., & Foreman, B. Z. (2018). Geomorphic stasis and spatiotemporal scales of stratigraphic completeness. *Geology*, *46*(4), 311–314. https://doi.org/10.1130/g40045.1

Straub, K. M., Paola, C., Mohrig, D., Wolinsky, M. A., & George, T. (2009). Compensational stacking of channelized sedimentary deposits. *Journal of Sedimentary Research*, *79*(9), 673–688. https://doi.org/10.2110/jsr.2009.070

Syvitski, J. P., & Milliman, J. D. (2007). Geology, geography, and humans battle for dominance over the delivery of fluvial sediment to the coastal ocean. *The Journal of Geology*, *115*, 1–19. https://doi.org/10.1086/509246

Tipper, J. C. (1983). Rates of sedimentation, and stratigraphical completeness. *Nature*, *302*(5910), 696–698. https://doi.org/10.1038/302696a0

Tipper, J. C. (2014). The importance of doing nothing: Stasis in sedimentation systems and its stratigraphic effects. *Geological Society, London, Special Publications*, *404*(1), 105–122. https://doi.org/10.1144/sp404.6

Tofelde, S., Savi, S., Wickert, A. D., Bufe, A., & Schildgen, T. F. (2019). Alluvial channel response to environmental perturbations: Fill-terrace formation and sediment-signal disruption. *Earth Surface Dynamics*, *7*(2), 609–631. https://doi.org/10.5194/esurf-7-609-2019

Tucker, G. E., & Slingerland, R. (1997). Drainage basin responses to climate change. *Water Resources Research*, *33*(8), 2031–2047. https://doi.org/10.1029/97wr00409

Tucker, G. E., & Whipple, K. X. (2002). Topographic outcomes predicted by stream erosion models: Sensitivity analysis and intermodel comparison. *Journal of Geophysical Research*, *107*(B9). https://doi.org/10.1029/2001jb000162

Turner, S. K. (2018). Constraints on the onset duration of the Paleocene-Eocene thermal maximum. *Philosophical Transactions. Series A, Mathematical, Physical, and Engineering Sciences*, *376*(2130), 20170082. https://doi.org/10.1098/rsta.2017.0082

Vacherat, A., Mouthereau, F., Pik, R., Huyghe, D., Paquette, J.-L., Christophoul, F., et al. (2017). Rift-to-collision sediment routing in the Pyrenees: A synthesis from sedimentological, geochronological and kinematic constraints. *Earth-Science Reviews*, *172*, 43–74. https://doi.org/10.1016/j.earscirev.2017.07.004

Vimpere, L., Spangenberg, J. E., Roige, M., Adatte, T., De Kaenel, E., Fildani, A., et al. (2023). Carbon isotope and biostratigraphic evidence for an expanded Paleocene–Eocene Thermal Maximum sedimentary record in the deep Gulf of Mexico. *Geology*, *51*(4), 334–339. https://doi.org/10.1130/g50641.1

Viviroli, D., Dürr, H. H., Messerli, B., Meybeck, M., & Weingartner, R. (2007). Mountains of the world, water towers for humanity: Typology, mapping, and global significance. *Water Resources Research*, *43*(7). https://doi.org/10.1029/2006wr005653

Westerhold, T., Marwan, N., Drury, A. J., Liebrand, D., Agnini, C., Anagnostou, E., et al. (2020). An astronomically dated record of Earth's climate and its predictability over the last 66 million years. *Science*, *369*(6509), 1383–1387. https://doi.org/10.1126/science.aba6853

Westerhold, T., Röhl, U., Donner, B., & Zachos, J. C. (2018). Global extent of early Eocene hyperthermal events: A new Pacific benthic foraminiferal isotope record from Shatsky rise (ODP site 1209). *Paleoceanography and Paleoclimatology*, *33*(6), 626–642. https://doi.org/10.1029/2017pa003306

Westerhold, T., Röhl, U., Laskar, J., Raffi, I., Bowles, J., Lourens, L. J., & Zachos, J. C. (2007). On the duration of magnetochrons C24r and C25n and the timing of early Eocene global warming events: Implications from the Ocean Drilling Program Leg 208 Walvis Ridge depth transect. *Paleoceanography*, *22*(2). https://doi.org/10.1029/2006pa001322

Westerhold, T., Röhl, U., Wilkens, R. H., Gingerich, P. D., Clyde, W. C., Wing, S. L., et al. (2018). Synchronizing early Eocene deep-sea and continental records – Cyclostratigraphic age models for the Bighorn Basin Coring Project drill cores. *Climate of the Past*, *14*(3), 303–319. https://doi.org/10.5194/cp-14-303-2018

Whipple, K. X., & Tucker, G. E. (1999). Dynamics of the stream-power river incision model: Implications for height limits of mountain ranges, landscape response timescales, and research needs. *Journal of Geophysical Research*, *104*(B8), 17661–17674. https://doi.org/10.1029/1999jb900120

Whitchurch, A. L., Carter, A., Sinclair, H. D., Duller, R. A., Whittaker, A. C., & Allen, P. A. (2011). Sediment routing system evolution within a diachronously uplifting orogen: Insights from detrital zircon thermochronological analyses from the South-Central Pyrenees. *American Journal of Science*, *311*(5), 442–482. https://doi.org/10.2475/05.2011.03

White, P. D., & Schiebout, J. (2008). Paleogene paleosols and changes in pedogenesis during the initial Eocene thermal maximum: Big Bend National Park, Texas, USA. *Geological Society of America Bulletin*, *120*(11–12), 1347–1361. https://doi.org/10.1130/b25987.1

Wing, S. L., Harrington, G. J., Smith, F. A., Bloch, J. I., Boyer, D. M., & Freeman, K. H. (2005). Transient floral change and rapid global warming at the Paleocene-Eocene boundary. *Science*, *310*(5750), 993–996. https://doi.org/10.1126/science.1116913

Zeebe, R. E., & Lourens, L. J. (2019). Solar System chaos and the Paleocene-Eocene boundary age constrained by geology and astronomy. *Science*, *365*(6456), 926–929. https://doi.org/10.1126/science.aax0612

Zhang, J., Covault, J., Pyrcz, M., Sharman, G., Carvajal, C., & Milliken, K. (2018). Quantifying sediment supply to continental margins: Application to the Paleogene Wilcox Group, Gulf of Mexico. *AAPG Bulletin*, *102*(09), 1685–1702. https://doi.org/10.1306/01081817308

References From the Supporting Information

Ardèvol, L. s., Klimowitz, J., Malagón, J., & Nagtegaal, P. J. C. (2000). Depositional sequence response to foreland deformation in the upper Cretaceous of the southern Pyrenees, Spain. *AAPG Bulletin*, *84*(4), 566–587. https://doi.org/10.1306/c9ebce55-1735-11d7-8645000102c1865d

Arévalo, O. J., Colombera, L., Mountney, N. P., Basilici, G., & Soares, M. V. T. (2022). Variations in water discharge at different temporal scales in a mud-prone alluvial succession: The Paleocene-Eocene of the Tremp-Graus Basin, Spain. *Sedimentary Geology*, *433*, 106122. https://doi.org/10.1016/j.sedgeo.2022.106122

Basilici, G., Colombera, L., Soares, M. V. T., Arévalo, O. J., Mountney, N. P., Lorenzoni, P., et al. (2022). Variations from dry to aquic conditions in Vertisols (Esplugafreda formation, eastern Pyrenees, Spain): Implications for late Paleocene climate change. *Palaeogeography, Palaeoclimatology, Palaeoecology*, *595*, 110972. https://doi.org/10.1016/j.palaeo.2022.110972

Cuevas, J. L. (1992). Estratigrafia del « Garumniense » de la Conca de Tremp. Prepirineo de Lérida. *Acta Geologica Hispanica*, *27*(1–2), 95–108.

Díez-Canseco, D., Arz, J. A., Benito, M. I., Díaz-Molina, M., & Arenillas, I. (2014). Tidal influence in redbeds: A palaeoenvironmental and biochronostratigraphic reconstruction of the lower Tremp formation (South-Central Pyrenees, Spain) around the Cretaceous/Paleogene boundary. *Sedimentary Geology*, *312*, 31–49. https://doi.org/10.1016/j.sedgeo.2014.06.008

IGME. (1959). *Monesma-1*. Instituto Geológico y Minero de España (IGME). Retrieved from https://info.igme.es/sigeof/

IGME. (1966). *Centenera*. Instituto Geológico y Minero de España (IGME). Retrieved from https://info.igme.es/sigeof/

IGME. (1968a). *Graus-1*. Instituto Geológico y Minero de España (IGME). Retrieved from https://info.igme.es/sigeof/

IGME. (1968b). *Santa-Creu-1*. Instituto Geológico y Minero de España (IGME). Retrieved from https://info.igme.es/sigeof/

IGME. (1975). *Cajigar-1*. Instituto Geológico y Minero de España (IGME). Retrieved from https://info.igme.es/sigeof/

Kiefer-Ollier, E., Loisy, C., & Cerepi, A. (2010). Diagenetic signature of the Mid-Paleocene exposure surface in the southeastern Pyrenean platform. *Comptes Rendus Geoscience*, *342*(6), 483–491. https://doi.org/10.1016/j.crte.2010.02.006

Oliva-Urcia, B., Gil-Peña, I., Samsó, J. M., Soto, R., & Rosales, I. (2018). A Paleomagnetic inspection of the Paleocene-Eocene thermal maximum (PETM) in the southern Pyrenees. *Frontiers in Earth Science*, *6*. https://doi.org/10.3389/feart.2018.00202

Owen, A., Ebinghaus, A., Hartley, A. J., Santos, M. G. M., Weissmann, G. S., & Mountney, N. (2017). Multi-scale classification of fluvial architecture: An example from the Palaeocene–Eocene Bighorn Basin, Wyoming. *Sedimentology*, *64*(6), 1572–1596. https://doi.org/10.1111/sed.12364

Pujalte, V., Schmitz, B., & Payros, A. (2022). A rapid sedimentary response to the Paleocene-Eocene Thermal Maximum hydrological change: New data from alluvial units of the Tremp-Graus Basin (Spanish Pyrenees). *Palaeogeography, Palaeoclimatology, Palaeoecology*, *589*, 110818. https://doi.org/10.1016/j.palaeo.2021.110818

Rosell, J., Linares, R., & Llompart, C. (2001). El « Garumniense » prepirenaico. *Revista de la Sociedad Geologica de Espana*, *14*(1–2), 47–56.

Schmitz, B., & Pujalte, V. (2003). Sea-level, humidity, and land-erosion records across the initial Eocene thermal maximum from a continental-marine transect in northern Spain. *Geology*, *31*(8), 689. https://doi.org/10.1130/g19527.1

Tremblin, M., Khozyem, H., Adatte, T., Spangenberg, J. E., Fillon, C., Grauls, A., et al. (2022). Mercury enrichments of the Pyrenean foreland basins sediments support enhanced volcanism during the Paleocene-Eocene thermal maximum (PETM). *Global and Planetary Change*, *212*, 103794. https://doi.org/10.1016/j.gloplacha.2022.103794